Metal–organic frameworks as semiconductors

Cláudia Gomes Silva, Avelino Corma* and Hermenegildo García*

Received 26th November 2009, Accepted 22nd December 2009
First published as an Advance Article on the web 22nd January 2010
DOI: 10.1039/b924937k

The aim of the present feature article is to present the current evidence in support of considering some MOFs as semiconductors. While MOFs and zeolites share common structural properties derived from the microporous crystal structure, zeolites are insulating materials and most of the attempts to exploit them in optoelectronics have met with failure. In contrast, some MOFs may have interesting photochemical properties that derive from the fundamental event of charge separation in electrons and holes upon light absorption. Photoinduced charge separation is the hallmark of a semiconductor that can behave simultaneously as an oxidizing or reducing agent. Considering the novelty of this field, most of the available data about MOFs as semiconductor have been obtained from MOF-5, a case that is complicated due to its low structural stability. Therefore, we point out that further studies showing the semiconducting properties of other MOFs are still welcome. The purpose of this feature article is to trigger intense research in this area including the synthesis of semiconducting MOFs by design and development of applications.

1. Properties of metal–organic frameworks compared to zeolites

Zeolites are microporous crystalline aluminosilicates whose structure is formed by SiO_4^{4-} and AlO_4^{5-} tetrahedra sharing the edges. These tetrahedra define channels and cavities perfectly regular of molecular dimensions termed micropores.[1–3] This intracrystalline empty space can be accessible from the exterior of the particle allowing mass transfer to the interior of the crystal. Depending on the dimensions of the pores, zeolites can be denoted as small, medium, large and extra-large pore sized when the channels are constituted by rings of 8, 10, 12 or more oxygens.[4,5] While small pore size can only adsorb molecules with diameters below 0.45 nm, the number of molecules that can access the interior of the particles in large pore zeolites is significantly larger.[6] In the case of medium pore size zeolites, the dimensions of the channels are similar to that of a benzene ring (around 0.54 nm). Typical pore diameter for large pore zeolites is about 0.74 nm though they can enclose cavities close to 1.5 nm.[7] Very recently new zeolites with pore diameters of 1.2 and 2.0 nm have been synthesized.[8,9] Fig. 1 shows the micropore geometries of zeolites ITQ-33 and ITQ-37.[8,10]

The importance of zeolites derives to a large extent from their use as adsorbents and solid acids particularly in large scale petrochemical processes.[6,11] Fig. 2 shows some of the catalytic industrial processes that are currently based on zeolites.[12]

Instituto de Tecnología Química, UPV-CSIC, Universidad Politécnica de Valencia, Avda. de los Naranjos s/n, 46022 Valencia, Spain

Cláudia Gomes Silva

Cláudia Gomes Silva was born in Porto (Portugal) in 1978 and graduated in Chemical Engineering at University of Porto in 2001. She got a MSc degree in Environmental Engineering in 2003 at the same university. She did her PhD studies on environmental photocatalysis under the supervision of Prof. Joaquim Luís Faria and graduated at University of Porto in 2008. She is now a postdoctoral fellow at the Institute of Chemical Technology, a joint centre between the Spanish National Research Council (CSIC) and the Technical University of Valencia. Her current research interests include materials science and photocatalysis.

Avelino Corma

Avelino Corma was born in Moncófar, Spain in 1951. He studied Chemistry at the Universidad de Valencia (1967–1973), and received his PhD at the Universidad Complutense de Madrid in 1976. He was a postdoc in the Department of Chemical Engineering at the Queen's University (Canada, 1977–1979). He has been director of the Instituto de Tecnología Química (UPV-CSIC) at the Universidad Politécnica de Valencia since 1990. His current research field is catalysis, covering aspects of synthesis, characterization and reactivity in acid–base and redox catalysis. He is co-author of more than 700 articles and 100 patents on these subjects.

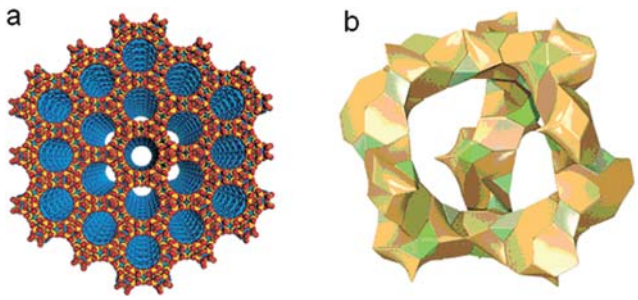

Fig. 1 Structures of zeolites ITQ-33 (a) and ITQ-37 (b).

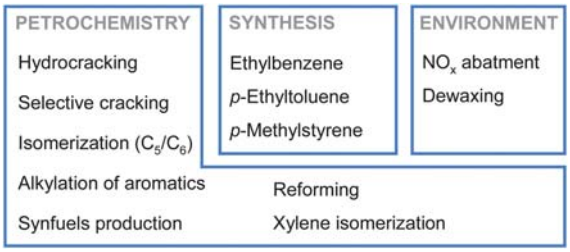

Fig. 2 Catalytic applications of zeolites in chemical industry.

With the advent of nanotechnology and nanoscience there was another line of research besides catalysis aimed at using zeolites as hosts to develop advanced materials where the presence of guests inside the zeolite micropores introduces a desired functionality or response in the solid. There are numerous reviews summarizing the use of zeolites as hosts for the preparation of novel materials with new properties as photocatalysts, electrodes, pigments, sensors and thermochromic materials, among other smart materials.[13–19] However, many applications of zeolites in the field of nanotechnology are hampered by the fact that aluminosilicates are wide bandgap insulators. For the occurrence of many interesting effects in the field of nanoscience it would be desirable that the host framework behaves as either a semiconducting or a conducting material. Typical applications of semiconductors include its use in solar cells and as photocatalysts. Moreover, the conducting properties of the host could eventually be useful to establish electronic contact between the external macroscopic electrodes and the occluded incorporated guest.

Hermenegildo García

Hermenegildo García (Herme) has been a full Professor and member of the Institute of Chemical Technology at the Technical University of Valencia since 1996. He has co-authored over 400 papers, supervised over 28 PhDs and holds 14 international patents. His main current interests are in green chemistry and catalysis as well as the use of zeolites, metal organic frameworks and mesoporous materials in supramolecular photochemistry, photocatalysis and nanotechnology.

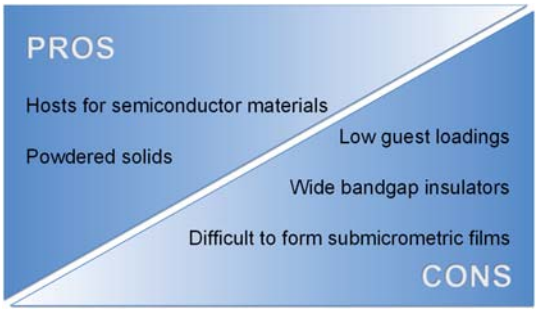

Scheme 1 Advantages and disadvantages of zeolites in nanotechnology.

However in the case of the zeolites their framework acts as an electrical insulator, impeding or making difficult the charge transport from or to the embedded guest and the working electrode. From the above considerations, it can be summarized that while zeolites are successful materials in heterogeneous catalysis and adsorption-separation they may be limited host materials for applications in those devices that require electronic response or charge transport through the zeolite. Scheme 1 summarizes the pros and cons of zeolites for developing nanoscience and nanotechnology.

In this context metal–organic frameworks (MOFs) may offer certain advantages for applications that need semiconducting properties. In this feature article we will describe that there is strong evidence showing that MOFs can be semiconductors and this property opens a new arena in nanoscience. A comprehensive review on all the literature in this field is out of the scope of the present work and we will concentrate mostly in our contribution to the development of this new area.

After a brief description of the most important structural properties of MOFs relevant to their semiconductor properties we will summarize those reports in which MOFs have been found to exhibit properties that can serve to develop devices and systems of nanometric dimensions. The reader should refer to recent reviews for a more detailed and comprehensive description of the synthesis,[20–22] structure[23–25] and general characteristics of MOFs.[26–32] For the sake of brevity and in order to avoid redundancy, we will limit ourselves to exemplify those properties of MOFs that derive from their use as semiconductors. Our goal is to stimulate future research in this area that can eventually lead to commercial applications of MOFs as semiconductors.

2. Structure of metal–organic frameworks

Metal–organic frameworks are a class of crystalline hybrid inorganic–organic materials whose crystal structure is made up of extended 3D networks of metal ions or small discrete metal clusters connected through multidentate organic spacers.[33–36] To be considered as a MOF, these building units should organize spatially in such a way that crystalline porous structures defining channels and cavities of regular size and shape on the nanometre scale are formed. The crystal framework of MOFs is analogous to that of zeolites and other related purely inorganic porous materials, but there are clear differences between them

concerning porosity, range of thermal and chemical stability, and feasibility of building a crystal structure by design. In particular, MOFs exhibit values of specific surface areas even above 3000 $m^2 g^{-1}$ and specific pore volumes as large as 1 $cm^3 g^{-1}$, which are among the highest values ever reported for any porous material. MOFs have an extremely wide-open structure in which the free space available for host molecules can reach even 90% of the crystal volume.[37] This results in the lowest framework densities attained so far for any crystalline material (a value as small as 0.21 g cm^{-3} has been reported for IRMOF-16).[37] Also in the case of MOFs it is possible to achieve fine control over the chemical environment and the topology of the internal voids by selecting appropriate building blocks (dimensions and functionalities of the organic linkers and size of the metal clusters) and the way in which they are connected. However, due to the presence of organic building blocks, MOFs are obviously much less stable than zeolites to thermal treatment, to the presence of chemical agents and even to moisture. One of the most common materials, denoted as MOF-5,[38] contains clusters of Zn_4O forming interconnecting structural nodes that are linked orthogonally to six units of terephthalate. Fig. 3 shows an illustration of the MOF-5 structure.

Since MOFs can be synthesized by design it would be of great interest to define which are the general structural requirements for having MOFs suitable for acting as semiconductors. Upon irradiation with photons of energy larger than their bandgap, a semiconductor must lead to a state of charge separation in which either the electron or the hole can easily migrate through the whole particle. Typical semiconductors such as TiO_2 have electrons in a conduction band constituted mainly by empty Ti *d* orbitals that expands throughout the particle. Considering that many MOFs have transition metals as structural nodes and that they are separated by the organic linkers, analogous conduction bands would require the effective mixing of empty *d* metal orbitals with the LUMOs of the organic linkers. Clearly computational calculations determining the density of states of the solids are necessary to delineate the requirements of metals and linkers for having this type of electronic conduction. These calculations will be of much help in understanding semiconduction in MOFs and to assist in the design of MOFs purposely synthesized as semiconductors.

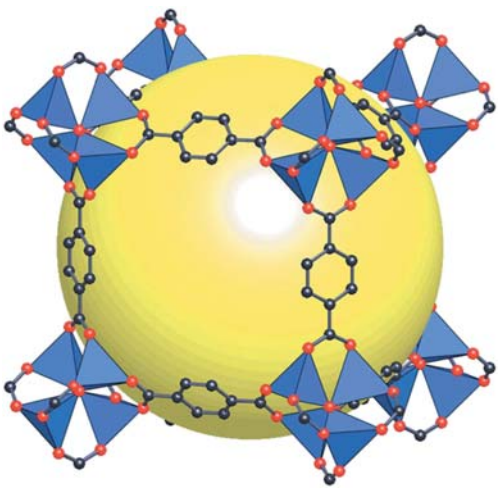

Fig. 3 The MOF-5 structure shown as ZnO_4 tetrahedra (blue polyhedra) joined by benzene dicarboxylate linkers (O, red and C, black) to give an extended 3D cubic framework with interconnected pores of 8 Å aperture width and 12 Å pore (yellow sphere) diameter. Yellow sphere represents the largest sphere that can occupy the pores without coming within the van der Waals size of the framework. (Figure taken from ref. 39 with permission.)

Photoinduced charge separation with the generation of electrons and holes is a transient state that decays typically in the submillisecond time scale returning to the neutral ground state through charge recombination. Charge annihilation can lead to an emissive state that can be detected and studied by monitoring the photoluminescence in addition to other photophysical techniques. For this reason photoluminescence can be a simple tool to determine the rate constant of charge recombination in those cases in which photon absorption produces charge separation that decays with emission. Photoluminescence of MOFs can also have applications in other fields such as sensors or emitting diodes.[40] In the following sections we will comment on how the observation of photoluminescence led initially to the proposal that MOFs can be semiconductors.

3. Photoluminescence of MOF-5

MOF-5 is the most-studied MOF with respect to its activity as a semiconductor. Absorption and emission spectroscopies are general and simple techniques to determine the relative energies of electronic excited states that are fundamental data related to the semiconducting properties.

There are conflicting reports in the literature about the origin of photoluminescence in MOFs. In some cases it has been proposed that the emission observed in MOFs is exclusively originated from the ligand rather than from the metal–ligand unit.[41,42] This proposal has been based on the lack of influence of the nature of metal ion (Zn, Be, Mg, Ca or Cd) on the emission from IRMOF-1.[41] Likewise, a 2D MOF Zn norfloxacine and another Cd MOF containing 5-sulfosalicylic acid (see structures in Scheme 2) were found to display an intense emission that is almost coincident with the emission of the free ligands and its metal complexes in solution.[42]

In contrast to these reports and particularly in the most widely studied case of MOF-5 it has been observed that the photoluminescence of the solid is different from that of the ligand or its carboxylated salts. As will be mentioned below, photoluminescence in MOF-5 and its hydrated derived phase is interpreted as arising from the unique interaction between the nodal

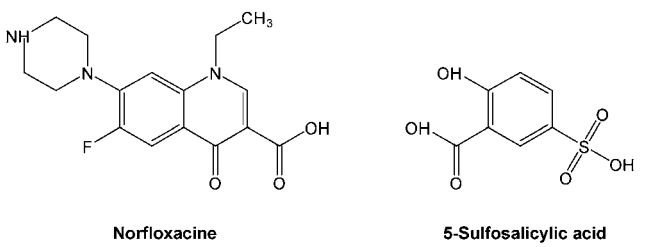

Scheme 2 Structures of norfloxacine and 5-sulfosalicylic acid.

metal clusters and the organic linker occurring exclusively in the "rigid" crystal structure of MOF.

Therefore, from the available data it can be concluded that there are two types of MOFs with respect to their photophysical properties depending on whether or not the metal–linker interaction and spatial structure of MOF results in specific electronic transitions. Considering the large number of possible MOFs in terms of the nature of metals and organic linkers the existence of these two extreme types of MOFs with respect to the photoluminescence properties (and possibly all the intermediate situations) is not surprising and simply reflects the existence of cases in which orbital overlap takes place leading to new electronic states. Obviously for observing semiconducting properties the occurrence of favorable orbital overlap is necessary. Therefore, we will concentrate here on those types of MOFs where the photochemical properties of the ligand are altered by interaction with the constitutional metal ions or clusters.

In a pioneering work, Bordiga, Zecchina and co-workers reported for the first time the photoluminescence of MOF-5.[43] As mentioned earlier when describing the structure of MOFs, MOF-5 is constituted by a cluster of Zn_4O in which there is a central oxygen atom connected to 4 Zn atoms (see Fig. 3). The subsequent coordination sphere of the cluster is defined by 12 oxygens from the organic linker. In this way, it can be considered that MOF-5 is constituted by Zn_4O_{13} clusters that can behave as quantum dots surrounded by 6 terephthalate ligands. These terephthalate ligands can act as antennae absorbing light from wavelengths longer than 220 nm. Analysis of the optical spectrum of MOF-5 shows contributions from both the organic linker and the Zn_4O_{13} centre. In this way, the authors suggested that MOF-5 can be considered as a zinc oxide-like quantum dot being sensitized by the aromatic ligand. Scheme 3 presents the idea of considering the constituents of MOF-5 behaving as independent quantum dots connected to an aromatic antenna.[43]

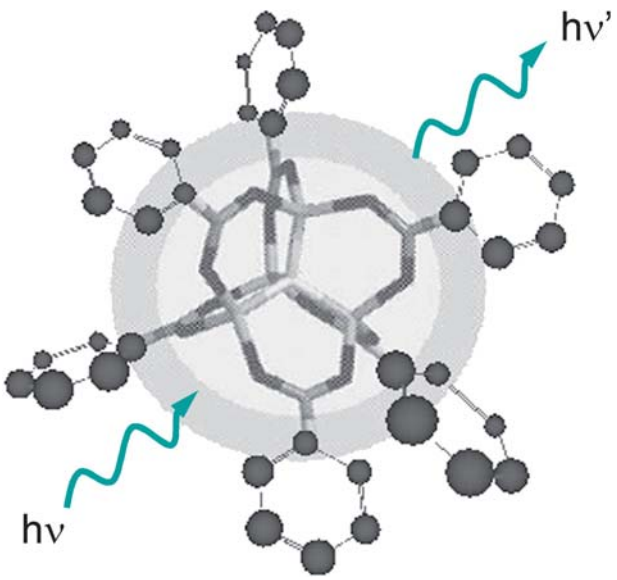

Scheme 3 Zn_4O_{13} group of MOF-5 Zn (light grey sticks) and O (dark grey sticks); benzene units acting as photon absorbers ($h\nu$) are able to efficiently transfer energy to the inorganic part where the photon emission occurs ($h\nu'$).

Consistent with the previous rationalization that MOF-5 is constituted by Zn_4O_{13} quantum dots, relatively strong photoluminescence was observed upon excitation of the MOF. Bulk ZnO exhibits very low photoluminescence emission characterized by a broad band centered at 560 nm (Fig. 4). The maximum intensity of ZnO emission occurs upon excitation at 380 nm. Actually ZnO follows a general behavior common for semiconducting metal oxides and particularly TiO_2.[44,45] Indeed, TiO_2 does not emit photoluminescence except for very small nanoparticles of size smaller than a few nanometres.

In contrast to the weak photoluminescence observed for ZnO, MOF-5 material emits from 450 to 650 nm, this emission being estimated as 16 times more intense than that of ZnO under the same conditions.[43] In addition, the emission of MOF-5 is significantly blue shifted with respect to that observed for ZnO. Interestingly, in MOF-5 the emission arising from the terephthalate units is not observed, this phenomenon being consistent with the operation in MOF-5 of an efficient energy transfer mechanism from the terephthalate singlet excited state to Zn_4O_{13} clusters.

The lifetime of photoluminescence obtained from the best fitting of the emission temporal profile in MOF-5 to a single exponential kinetics was estimated as 600 ns.[46] This emission lifetime is remarkably long and certainly unusual for fluorescence from organic compounds that typically is at most a few nanoseconds.[47] Previous studies on the decay kinetics of TiO_2 clusters inside zeolites have shown complex decays but reaching similar values to those observed for the emission in MOF-5. Probably, the single exponential kinetics is a manifestation of the crystal structure and identical environments for Zn_4O_{13} in MOF-5 (single site).[46] In contrast, the multi-exponential decay observed for nanoclusters of TiO_2 in zeolites indicates a distribution of lumophores among different populations, probably related to the lack of uniformity in the composition and size of the TiO_2 clusters.[48]

The influence of the temperature on the photoluminescence intensity and its comparison with the behavior of ZnO nanoparticles provides some insight into the barrier energy of trapped electrons in both semiconductors.[49] It was estimated that in ZnO some electrons are trapped from 50 to 190 meV below the conduction band edge probably in structural defects consisting

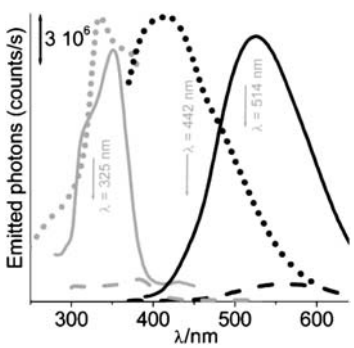

Fig. 4 Photoluminescence spectra of MOF-5 and ZnO nanoparticles. Grey curves (excitation scans), black curves (emission scans). MOF-5 (solid, $\lambda_{em} \sim 518$ nm and $\lambda_{ex} \sim 350$ nm); terephthalic acid disodium salt (dotted, $\lambda_{em} \sim 418$ nm and $\lambda_{ex} \sim 335$ nm); ZnO (dashed, $\lambda_{em} \sim 560$ nm and $\lambda_{ex} \sim 380$ nm). (Figure taken from ref. 43 with permission.)

of oxygen vacancies.[50] To observe photoluminescence arising from these trapped electrons the activation energy is 80 meV. Similar studies with MOF-5 show that the intensity of the photoluminescence spectrum first decreases up to 170 K and then increases in the 170–110 K range. To interpret this abnormal behavior it is necessary to assume the presence of an activation energy for the thermal non-radiative decay of 120 meV as well as a second characteristic energy (E_c) of 5 meV. The higher activation energy of the non-radiative decay indicates that electrons in MOF-5 are more strongly trapped than in ZnO. However, the origin of the E_c of MOF-5 is unclear and requires further studies to be interpreted. From the dependence of maximum emission wavelength shift and emission band width on temperature it can be concluded that the photoluminescence observed for MOF-5 nanoparticles arises from charge recombination occurring between deeply trapped charges, *i.e.*, localized electrons and holes.[49] Fig. 5 shows the influence of temperature on the photoluminescence of ZnO and MOF-5.

The temperature at which the photoluminescence is measured also determines the width of the emission band. By measuring the bandwidth at different temperatures for MOF-5 and ZnO, it was quantitatively established that the reorganization energy of the charge separated state in MOF-5 is about 1.6 times larger than for ZnO. This could be a reflection of the crystal structure of MOF-5 and of the nature of the electron donor and acceptor moieties involved in the process of charge separation. As conclusion, it appears that comparison of the photoluminescence activation energy and reorganization energy indicates that in the case of MOF-5 the charge separation state is more deeply trapped and produces larger structural changes than in ZnO, the closest related semiconductor with which to compare the behavior of MOF.

The previous observation of MOF-5 photoluminescence and its interpretation constitutes a seminal contribution triggering the quest for electroptical applications in MOFs and particularly those that are characteristic of semiconductors and quantum dots. As mentioned earlier in the introductory section, zeolites that in many fields have superior properties and performances than MOFs can never be considered as semiconductors and at most they can be inert solid hosts to incorporate photoactive guests. For instance, while pure zeolites and related aluminosilicates do not absorb UV radiation of wavelengths longer than 220 nm, the onset of the MOF-5 absorption band appears at 450 nm and, obviously, absorption of light in the visible region of the electromagnetic spectrum can be tuned in MOFs by the choice of appropriate metal clusters and/or organic linkers.

4. Electron transfer photoluminescence quenching

Systematic quenching studies of the photoluminescence of MOF-5 particles in the presence of a series of electron donors have been carried out with the aim of comparing the quenching behavior with that observed for nanoparticulate ZnO as a related material.[49] This comparison should provide information about the similarity/dissimilarity between MOF-5 and ZnO.

It was observed that in general there is a relationship between the oxidation potential of the quencher and the quenching rate constant of MOF-5 photoluminescence. As can be seen in Fig. 6 the quantitative behavior of photoluminescence quenching for MOF-5 nanoparticles and ZnO follows a similar trend for most quenchers. However, there are some clear differences for those quenchers that are strongly adsorbed in MOF-5, such as 4-(methylthio)phenylacetic acid and 4-(methylthio)phenylmethanol. Even more remarkable is the case of 4-phenylbenzoic acid for which a high value of quenching rate constant was measured for MOF-5 even though the oxidation potential is as high as +2.3 V *versus* NHE. It could be that in those cases where

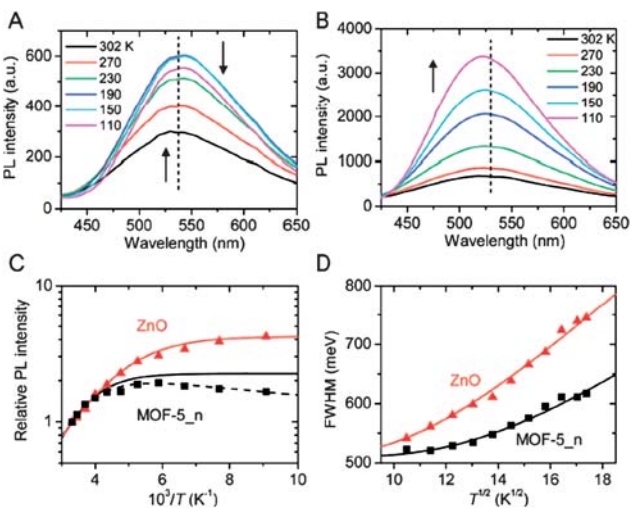

Fig. 5 Photoluminescence (PL) spectra of nanoparticulate MOF-5 (MOF-5_n) (A) and ZnO (B) powders under N_2 atmosphere at different temperatures. Temperature dependences of the relative photoluminescence intensity (C) and FWMH (D) observed for MOF-5_n (black squares) and ZnO (red triangles) powders. (Figure taken from ref. 49 with permission.)

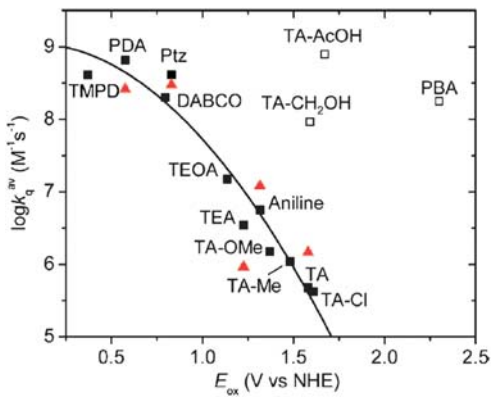

Fig. 6 Relationship between the oxidation potential (E_{ox}) of the quencher and log k_q^{av} (k_q^{av} is the average quenching constant) obtained for MOF-5 nanoparticles (black squares) and ZnO (red triangles). The open squares, which are obtained for MOF-5 particles, significantly deviate from the tendency obtained for other quenchers due to surface adsorption. Codes: Thioanisole, TA; *p*-methylthioanisole, TA-Me; *p*-chlorothioanisole, TA-Cl; *p*-methoxythioanisole, TA-OMe; 4-(methylthio)phenylmethanol, TA-CH_2OH; 1,4-phenylenediamine, PDA; *N*,*N*,*N*′,*N*′′-tetramethyl-*p*-phenylenediamine, TMPD; 4-(methylthio)-phenylacetic acid, TA-AcOH; 4-phenylbenzoic acid, PBA; triethylamine, TEA; triethanolamine, TEOA; 1,4-diazabicyclo[2.2.2]octane, DABCO; phenothiazine, Ptz. (Figure taken from ref. 49 with permission.)

adsorption inside MOF-5 is very strong, a pre-concentration of the quencher inside MOF-5 micropores enhances remarkably the quenching efficiency. Therefore, in those cases, the large porosity and adsorption capacity characteristic of MOF materials will play a role in the photochemical process.

5. Photoluminescence of other MOFs

Besides Zn terephthalate, the photoluminescence of other Zn MOFs, namely zinc *trans*-4,4′-stilbene dicarboxylate MOF, has been studied by Allendorf and co-workers.[51] It was found that the solvothermal reaction of Zn nitrate and *trans*-4,4′-stilbene dicarboxylic acid can render two different materials depending on the solvent and the conditions used for the material preparation. Working in *N*,*N*-dimethylformamide at temperatures between 70 and 85 °C a layered MOF is obtained. In contrast, similar reaction using *N*,*N*-dimethylformamide at 105 °C affords a different crystal structure constituted by two interpenetrating cubic lattices also featuring Zn carboxylate linkages. This 3D structure is analogous to isoreticular MOF. Fig. 7 illustrates the crystal structures of the two materials containing Zn stilbene carboxylate bonds and differing in the dimensionality and geometry of the framework. Interestingly, both solids contain the Zn_4O nodes that are also present in MOF-5 and that are believed to be responsible for the solid photoluminescence.

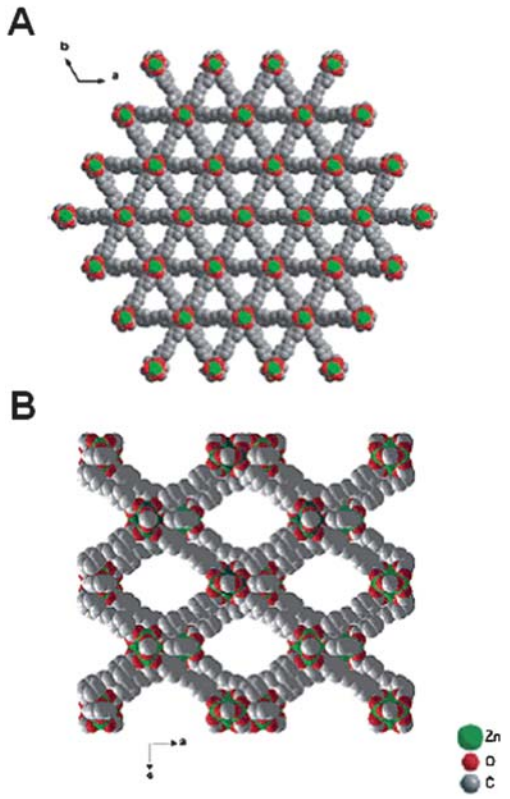

Fig. 7 A. Space-filling model showing the 2D network formed from $Zn(NO_3)_2$ and *trans*-4,4′-stilbene dicarboxylate at 70–85 °C in DMF; B. [011] projection showing the pores extended through the 3D crystal obtained with the same precursor at 105 °C. (Figure taken from ref. 51 with permission.)

Both solids exhibit an intense structured fluorescence with vibronic features upon UV illumination, but differ in the spectra. The emission spectrum of an individual crystal of the 3D material is coincident in the band position with that recorded for diluted solutions of *trans*-stilbenecarboxylate in DMSO/water (100 : 1) suggesting no influence of the Zn_4O clusters on the emission. In contrast, the emission spectrum of the layered Zn stilbene carboxylate material is much broader and significantly red shifted. Also the two solids differ in the peak position and bandwidth of the excitation spectra. Fig. 8 shows normalized excitation and emission spectra of the two Zn stilbene solids.

The differences in the photoluminescence spectra of these two Zn stilbene MOFs have been attributed to the differences in the ligand–ligand interaction rather than to differences arising from the interaction of the ligands with the Zn_4O clusters common for the two solids as well as for MOF-5. This interpretation of the different photoluminescence spectra was based on precedents in which the emission of MOFs was found to be very similar to

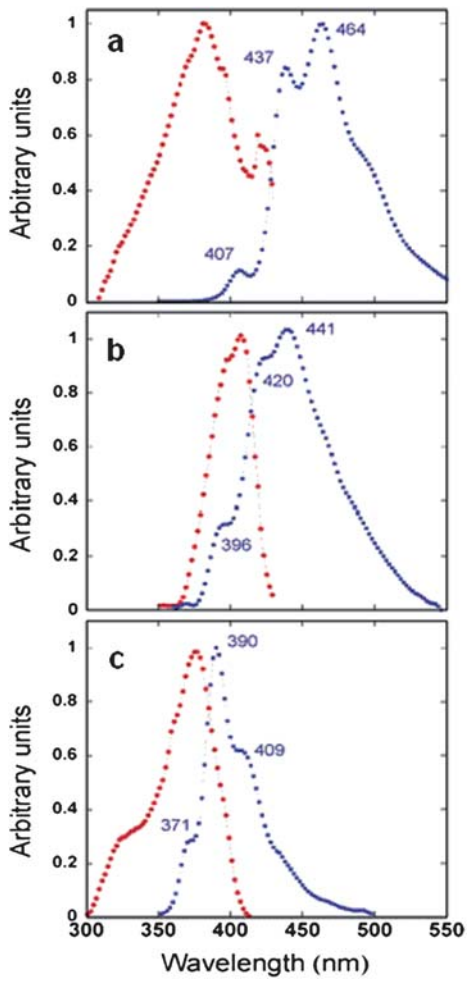

Fig. 8 Normalized excitation (red circles) and emission (blue squares) spectra for: a) *trans*-4,4′-stilbene dicarboxylic acid; b) 2D network; c) 3D framework structure. Spectra b) and c) were obtained for individual crystals soaked in $CHCl_3$. $\lambda_{ex} = 350$ nm for spectra a) and b), 325 nm for spectrum c). Emission maxima for the first three vibronic bands are indicated. Excitation spectra were recorded monitoring at 450 nm. (Figure taken from ref. 51 with permission.)

those of the ligand and independent from the nature of the metal.[41–43,52] Also some theoretical calculations by DFT indicate that the highest occupied valence levels are dominated by the p orbitals of the aromatic carbon atoms with negligible contribution from the carboxylate substituent that is interacting with the Zn_4O clusters.[53] In a simplistic interpretation, the theoretical model indicates that in these stilbene MOFs, the photoluminescence is localized on the stilbene chromophore without interaction with the metal clusters.

Thus, the interchromophore interaction due to interligand π–π complexation occurring in the 2D layered MOF but not in the 3D MOF will be the main cause of the remarkable differences of the photoluminescence of the two materials based on Zn *trans*-stilbene dicarboxylic acid. This proposal is in agreement with the observation in the emission spectrum of several vibronic bands in the photoluminescence of the 2D and 3D zinc stilbene MOFs. Observation of structured emission is a typical feature of aromatic organic compounds. Also, this fine structure of the emission rules out the contribution of excimer emission to the spectra, as could have been predicted based on the chromophore distances in the crystal structures of the two Zn *trans*-stilbene carboxylate. It is well known that excimer emission is characterized by a featureless broad band.[47]

One interesting point that deserves some comment is the fact that the difference in the wavelength maximum between the excitation and emission peaks in the Zn stilbene dicarboxylate MOFs (1215 cm^{-1} for the 2D and 815 cm^{-1} for the 3D MOFs) is significantly smaller than for the same ligand in diluted dioxane solution (3400 cm^{-1}). This indicates that the degree of reorganization between the ground and first singlet excited states of the *trans*-stilbene chromophore in the Zn MOFs has been significantly reduced as compared to solution. This has been interpreted as a reflection of the increased rigidity of the stilbenoid unit when incorporated in the MOF framework as compared to the solution. As indicated in Scheme 4, after light absorption and generation of the singlet excited state, the geometry of this electronically excited state may differ from that of the ground state. Therefore, when the stilbene chromophore is in a flexible environment like in solution, it undergoes geometrical relaxation in the electronic excited state potential energy surface to a more stable conformation and this relaxation energy loss is reflected later in a lower energy of the emitted fluorescence. Apparently when coordinated to the Zn^{2+} ions in MOF, the coordinative interaction with these metal ions impedes the geometrical relaxation occurring in solution.

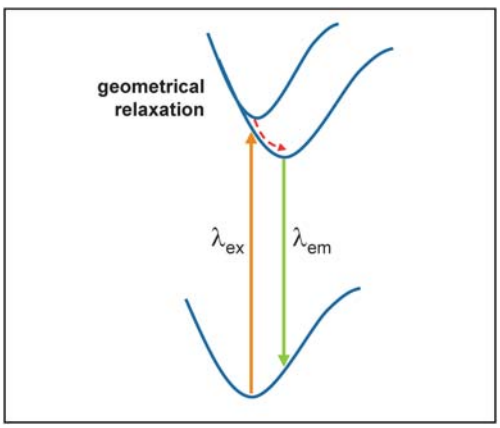

Scheme 4 Energy diagram showing the origin of the Stokes shift between the emission and excitation wavelengths as a consequence of the conformational relaxation in the excited state. Light absorption and emission correspond to the vertical transition between potential energy surfaces. Note the difference in energy and wavelength between excitation and emission.

Time resolved emission measurements were also used to gain insight into the local environment and rigidity of the stilbenoid units in MOF crystals. The emission lifetime of *trans*-stilbene in solution is very short (<100 ps) due to the ease of *trans–cis* isomerisation arising from the barrierless rotation around the central double bond in the first excited state. Also the fluorescence quantum yield of *trans*-stilbene in solution is very low ($\phi_{fl} \sim 0.02$ in acetonitrile). In contrast, when forming part of the MOF structure the lifetime of the emission increases, probably also as a consequence of the increased rigidity of the coordinated stilbenoid chromophore. These variations in the emission lifetime and quantum yield are a direct consequence of the immobilization of the photolumophore in a rigid crystal framework.

Another interesting observation that could be the basis for sensor development is that the emission of crystals of 3D Zn stilbene MOF is sensitive to the nature of the guest solvent molecules, λ_{em} increasing in the order hexane, chloroform, toluene. These changes were found to be fully reversible through multiple cycles of solvent exchange, which is a pre-requisite for a suitable sensing material. In contrast, the Zn stilbene dicarboxylate lacking three-dimensional structure is insensitive to the interaction with guest molecules, probably because the π-stacking of the stilbene linkers impedes interaction and solvation by the organic liquids.

The above example serves to illustrate those cases in which the photoluminescence of MOFs arises from excitons localized exclusively on the organic linker without interaction with the metal ions or clusters. Most likely these types of MOFs in which no semiconducting behavior (photoinduced electron transfer between the linker and the metal ion or cluster) is observed are those in which the organic linker has a low lying electronic excited state.

6. Use of photoluminescent MOFs as sensors

An intermediate situation between the type of MOFs with photoluminescence localized on the organic linker and those behaving as semiconductors are lanthanide MOFs. Lanthanides (Lns) are well known for their unique photoluminescence emission in the visible arising from relaxation of atomic electronic excited states.[54] This photoluminescence from lanthanides has been used in many applications including lasing, telecommunications, sensing and others.[32,55–60] The main problem of lanthanide photoluminescence is the small cross-section of lanthanide atoms for visible light absorption. This limitation has been frequently circumvented by the so-called antenna effect in which an organic chromophore absorbs initially the UV or visible light and subsequently transfers the energy to the atomic electronic states of the lanthanide atoms and ions.[61] This energy transfer from the antenna to the lanthanide is frequently much more efficient than the direct excitation of lanthanide atoms and ions.

In this context, MOFs containing lanthanides are very promising materials because the organic linker can act as an antenna producing the efficient photosensitization of the lanthanide acting as constitutional nodes of the metal framework. For this reason the synthesis of Ln MOFs has attracted considerable attention since the initial work in this area.[62–66]

One example of rare-earth MOFs are those containing 1,5- or 2,6-naphthalenesulfonates as linkers and La, Nd, Pr, Sm and Eu as lanthanides.[67] The paradigmatic case that has been studied in most detail is the Nd^{3+}-containing naphthalenesulfonate MOF. In this case it has been found that the optical absorption spectrum contains the characteristic narrow absorption peaks corresponding to the atomic transitions together with a broad, considerably more intense absorption band spanning into the UV region due to the organic linker (Fig. 9). As expected these materials exhibit the characteristic photoluminescence spectrum of Nd^{3+} upon exciting on the atomic absorption of Nd^{3+}.

In a more detailed study of the properties and potential applications of Ln MOF emission, a series of 3D MOFs using 4,4′-(hexafluoroisopropylidene)-bis(benzoic acid) as ligand was used (see structure in Scheme 5).[58] This ligand was selected on purpose because its high fluorine content should render the internal pores remarkably hydrophobic and insensitive to moisture and water.

The crystal structure of these fluorinated MOFs consists of a series of parallel nona- and octa-coordinated Ln chains held in place by the carboxy groups of the ligands (Fig. 10). The resulting material, when outgassed to remove solvent molecules,

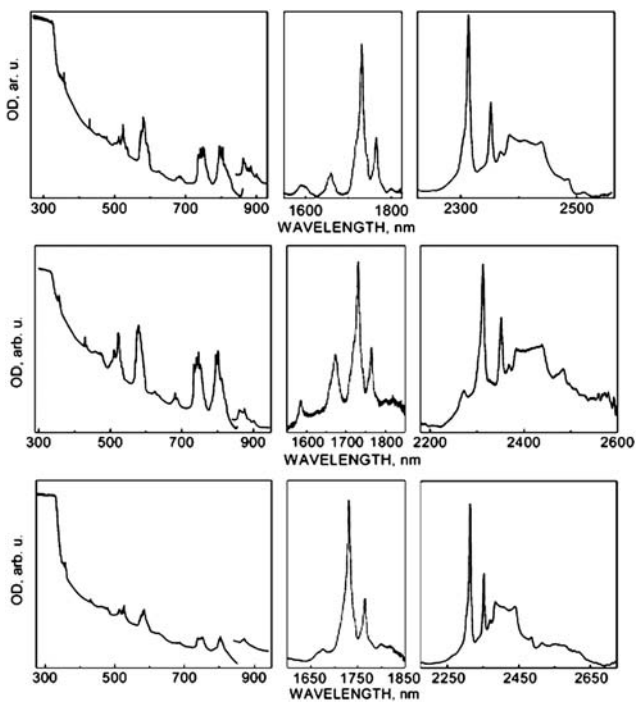

Fig. 9 Room-temperature optical absorption spectra (left column) and emission spectra (central and right columns) for Nd^{3+} MOFs: 3D structured MOF containing 1,5-naphthalenedisulfonic acid as linker (top); 2D structured MOF containing 2,6-naphthalenedisulfonic acid as linker (middle); 3D structured MOF containing 2,6-naphthalenedisulfonic acid as linker (bottom). (Figure taken from ref. 67 with permission.)

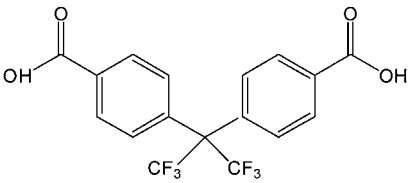

Scheme 5 Structure of 4,4′-(hexafluoroisopropylidene)-bis(benzoic acid).

gives a surface area of 207 $m^2\ g^{-1}$ which is the top of the range for Ln materials. For this family of Ln MOFs, materials with isomorphic substitution in various proportions of different Ln can be prepared. Thus, for example, a series of Ln MOFs containing simultaneously Eu and Gd in a range of atomic ratios from 5/95 to 66/34 have been described.[58]

Ln MOFs with 4,4′-(hexafluoroisopropylidene)-bis(benzoic acid) as ligand crystallize in long needles that can be handled individually. By placing one of these Ln MOF crystals parallel or perpendicular to the detector it has been determined that these MOFs exhibit a strong anisotropic photoluminescence. Thus, it was observed that the intensity of the emission bands upon excitation of the linker at 290 nm varies strongly depending on the orientation of the crystal (Fig. 11). This fluorescence anisotropy is a consequence of the alignment of all the chromophores in a preferred direction and proves that the crystallization as long needles is a manifestation of the ordering at the molecular level.

Concerning the antenna effect it has been determined that the quantum yield of photoluminescence upon excitation of the ligand is 0.48 that indicates a very efficient ligand-to-metal energy transfer as well as high emission yield. This quantum yield value for the antenna effect is a remarkably high number indicating that the energy transfer is very efficient.

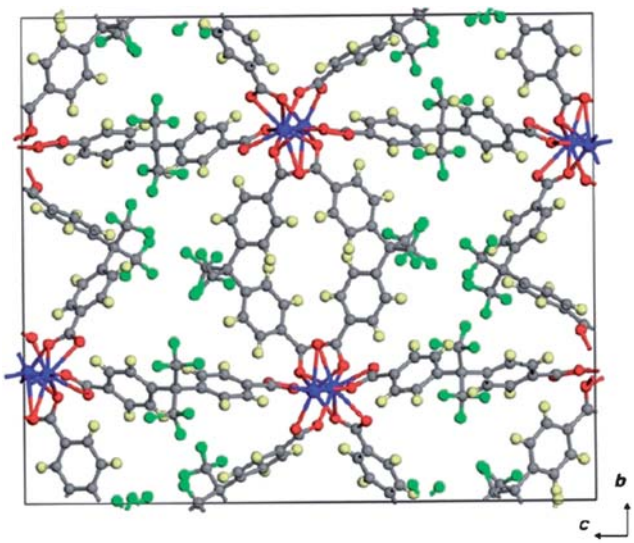

Fig. 10 Structure of ITQMOF-2 that contains lanthanide ions connected by 4,4′-(hexafluoroisopropylidene)-bis(benzoic acid) units (Eu blue, O red, C gray, F green, H yellow). (Figure taken from ref. 58 with permission.)

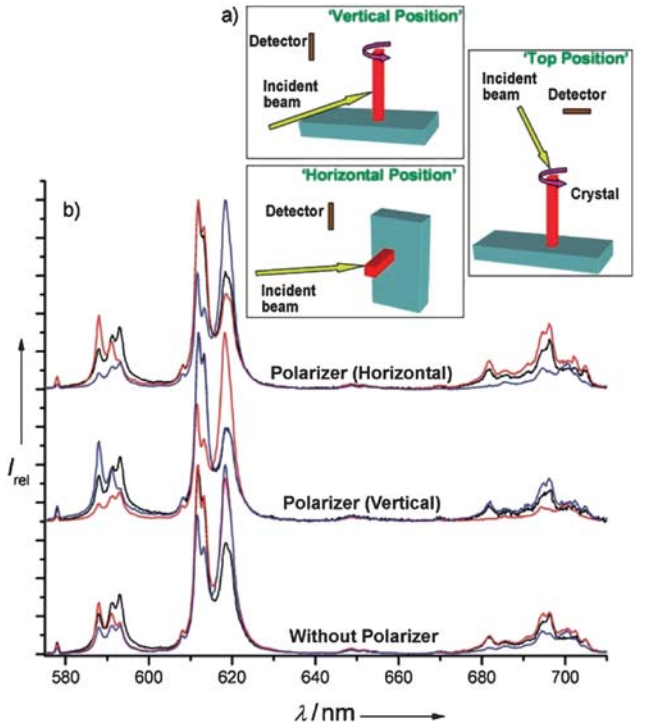

Fig. 11 a) Experimental setup and single-crystal orientations *versus* the detector. Note that the main difference between the "vertical" and "horizontal" positions is that in the former the plane of the detector and Xe light source are parallel to the crystal support, while in the latter position the plane of the detector and the Xe lamp are perpendicular to the support. b) Room-temperature emission spectra of a lanthanide (5Eu–95Gd) MOF single crystal, recorded using a polarizer just before the detector, for the three different crystal orientations (black line: top, red line: vertical, blue line: horizontal). The excitation was performed at 290 nm. (Figure taken from ref. 58 with permission.)

In the context of the present review, Ln MOFs represent an intermediate case between MOFs behaving as semiconductors and those in which the emission derives from the organic linker. In the case of Ln MOFs the interaction between the linker and the rare earth ion is well evidenced and firmly supported. Quantification of this interaction indicates that it is very efficient compared to other systems. However, while the mechanism of linker–metal interaction in semiconductors should be electron transfer, in the case of Ln MOFs the interaction is energy transfer and does not lead to charge separation.

7. Spectroscopic evidence of charge separation in MOFs by transient absorption spectroscopy

Laser flash photolysis is a powerful photochemical technique to record time-resolved absorption spectra of electronic excited states, states of charge separation and transient species generated after a laser beam pulse considered instantaneous on the time scale being monitored.

In the case of TiO_2, laser flash photolysis has allowed the detection of the photogeneration of electron and holes at picosecond time scale.[68] In the case of small TiO_2 clusters encapsulated inside zeolites there is a population of species derived from

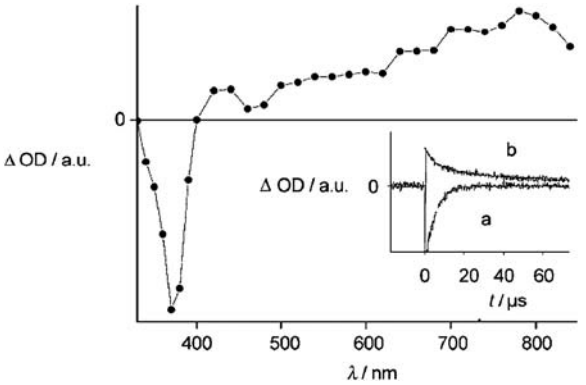

Fig. 12 Time-resolved diffuse reflectance UV/Vis spectrum of a N_2-purged sample of MOF-5 recorded 3 μs after 355 nm laser excitation. The inset shows the temporal profiles of the transient spectrum monitored at a) 370 nm and b) 780 nm. (Figure taken from ref. 46 with permission.)

charge separation that live longer than microseconds after the laser pulse.[48]

Laser flash photolysis of MOF-5 upon 355 nm laser excitation has allowed the detection of transient absorptions decaying in a few microseconds. Fig. 12 shows the transient spectrum recorded for MOF-5, 3 μs after the 355 nm laser pulse.[46] As can be seen, the spectrum is dominated by a continuous absorption peaking at the far red of the available wavelength region. An additional sharp negative signal at 370 nm attributable to the instantaneous bleaching of the MOF-5 ground absorption is also observed. The temporal profiles of the signal monitored at 370 and 780 nm show identical rate constants and inverse symmetric traces indicating that the species responsible for absorption at 780 nm decays to the ground state regenerating the depleted ground state. In addition, the temporal profiles of the signal monitored from 500 to 840 nm are identical which has been interpreted as an indication that the absorption band from 500–840 nm corresponds to a single transient species. A detailed kinetic analysis of the temporal profile at 780 nm shows that the signal fits a two first-order kinetics with lifetimes of 5 and 30 μs, respectively.

The assignment of the transient to electrons was based on quenching studies. This kinetic feature of the transient decay has been rationalized assuming that the band has contributions of two families of electrons in two different environments. The shortest lived electrons were attributed to the electrons localized on the Zn_4O_{13} cluster neighboring the ligand from where the electron has migrated. The longest lived electrons would correspond to the population of electrons that have migrated further away from the terephthalate ligand that has originated the photoinduced electron ejection. This interpretation parallels the classical studies in geminate and free radicals and radical cations that have shown that lifetimes are extremely dependent on the distance at which the two reacting transients (electrons and holes in our case) are separated.[47] Scheme 6 summarizes the proposal to rationalize the transient spectra and the signal kinetics detected by laser flash photolysis on MOF-5.

To better understand the photochemical process occurring in MOF-5 and determine its specificity with respect to their components, a study of the photochemistry of terephthalate

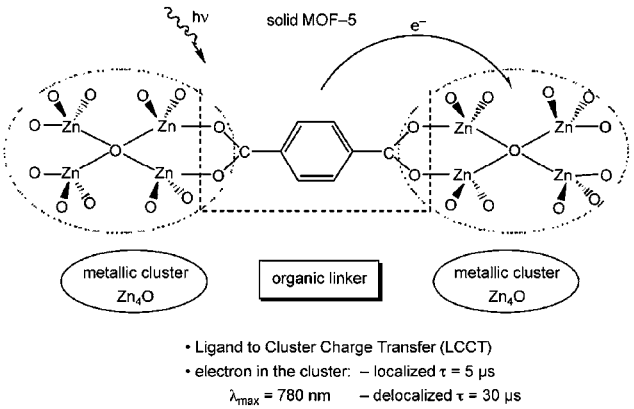

Scheme 6 Photophysical processes that occur after the irradiation of the MOF-5 solid material and an aqueous solution containing the terephthalate unit and Zn^{2+}.The differences between these two systems will be mainly in the kinetics and lifetimes of charge separation, arising from the rigidity of the crystal structure on MOF-5 as opposed to freely-diffusing species in solution.[46]

aqueous solutions in the absence and in the presence of Zn^{2+} was carried out.[46] Although MOFs are solid crystalline materials, insight into their properties can be obtained by studying the intrinsic properties of the ligands in the presence of the metal ions. With respect to this situation in homogeneous phase, the spatial structuring, ordering and rigidity occurring in the solid crystal can alter the photochemical behavior of MOFs. Thus, when terephthalate is photolysed in water, laser flash photolysis allows detection of the corresponding triplet at 300 and 400 nm of the aromatic dicarboxylate together with the solvated electrons that appear as an absorption starting at 750 nm and extending to the near infrared region. Fig. 13 shows the transient spectrum recorded for terephthalate in water.

Upon addition of Zn^{2+} ions, both signals corresponding to the triplet excited state of terephthalate and solvated electrons decrease in the initial intensity value at zero time and the residual signal decays faster. These two features (lower intensity and faster decay) are indicative of the simultaneous influence of static

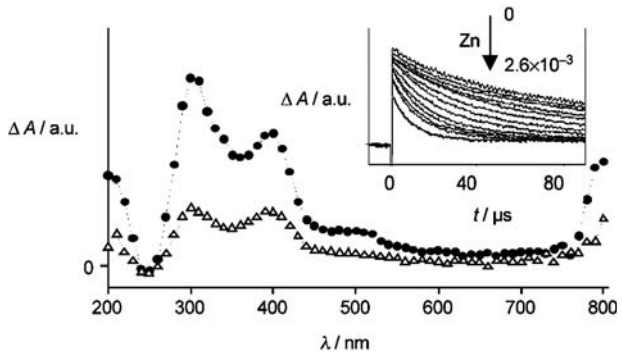

Fig. 13 UV/Vis transient absorption spectra of a N_2-purged aqueous solution of sodium terephthalate (1.1×10^{-4} M) recorded 4 μs after 266 nm laser excitation before (●) and after (△) the addition of an aqueous solution of Zn^{2+} (2.6×10^{-3} M). The inset shows the temporal profiles of the signal monitored at 400 nm recorded for a N_2-purged aqueous solution of sodium terephthalate upon addition of increasing amounts of Zn^{2+} from 0 to 2.6×10^{-3} M.[46]

and dynamic quenching of photoexcited terephthalate by Zn^{2+}. The static quenching indicates that there is a pre-association of terephthalate and Zn^{2+} in the ground state and upon photoexcitation of these aggregates instantaneous quenching occurs leading to a decrease in the signal intensity recorded immediately after the laser pulse. On the other hand the fact that the signal decay becomes faster with the concentration of Zn^{2+} indicates that those photoexcited terephthalates that during their lifetime encounter Zn^{2+} ions would undergo deactivation. The last process requiring diffusion is denoted as dynamic quenching. Overall the results of the laser flash photolysis in aqueous solution indicate that the presence of Zn^{2+} strongly influences the behavior of photoexcited terephthalate and that solvated electrons are trapped by Zn^{2+} acting as electron traps. Considering that MOF-5 has the same building blocks but in a rigid position, it is not unreasonable to assume that similar types of interactions but with increasing prevalence of static quenching will occur in MOF-5 compared to the experiment in aqueous solution.

Actually, the MOF-5 crystal structure can be considered as a periodic fixed repetition of Zn^{2+} cations interacting with terephthalate ligands. According to this observation of electron transfer quenching of terephthalate excited states by Zn^{2+} ions, the photoluminescence reported by Zecchina and co-workers could arise from the collapse of the singlet charge separation state.[43] Alternatively, long distance charge separation will produce longer-lived non-geminated transients that will be the species detected by transient spectroscopy. What is important for our purpose here is that the occurrence of long-lived charge separation would indicate that the MOF-5 structure acts as semiconductor allowing delocalization of some of the electrons/holes generated in the photoinduced electron transfer.

As mentioned earlier when commenting on photoluminescence quenching, the mechanism of photoluminescence deactivation by quenchers differing in the oxidation potential was proposed to be electron transfer.[49] To confirm that photoluminescence quenching occurs indeed through electron transfer from the quencher to the electron hole in MOF-5, laser flash photolysis studies of MOF-5 in the presence of thioanisole acetic acid were carried out, whereby the characteristic band at 450–660 nm corresponding to the thioanisole acetate radical cation was recorded immediately after the laser pulse. Moreover, the intensity of this peak increases as the MOF-5 suspension in acetonitrile contains larger amounts of thioanisole acetate.[49]

One remarkable detail that can be used to assess the activity of MOF-5 as semiconductor was obtained by laser flash photolysis monitoring the intensity of the transient signal at zero time corresponding to the wavelength of the maximum intensity of thioanisole acetate radical cation. In these experiments a 355 nm excitation wavelength was used and a comparison between the concentration of thioanisole acetate radical cation generated photochemically by exciting MOF-5 or P25 TiO_2 was obtained.[49] It has to be noted that at this laser wavelength the absorbance of P25 TiO_2 powder in acetonitrile is about 5 times higher than the absorbance of MOF-5 and therefore these conditions are unfavorable for MOF-5 with respect to excitation of P25 TiO_2. Nevertheless, it was observed that MOF-5 generates a larger initial concentration of thioanisole acetate radical cation (about 1.3 times higher than P25 titania). Moreover, in addition to the higher relative efficiency it is also remarkable that the lifetime of

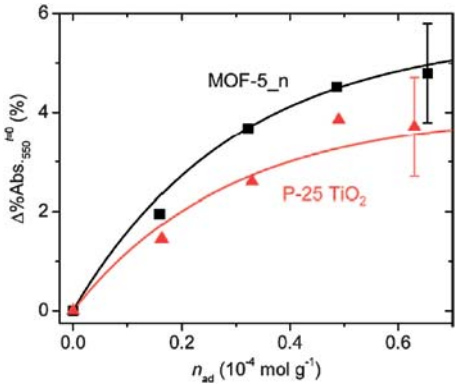

Fig. 14 Relationship between the initial transient signal intensity ($\Delta\%Abs^{t=0}$) obtained at 550 nm and the concentration of 4-(methylthio)phenylacetic acid (n_{ad}) detected upon 355 nm laser flash of suspensions of MOF-5 nanoparticles and P25 TiO_2. (Figure taken from ref. 49 with permission.)

the charge separated state is considerably longer for MOF-5 (over 15 μs) compared to that of P25 TiO_2 (about 5 μs). Fig. 14 illustrates the differences in the transient signal characteristic of 4-(methylthio)phenylacetic acid when photolysed in the presence of MOF-5 or P25. It is proposed that the observed long lifetime for MOF-5 nanoparticles arises from the slow motion of electrons in the particles due to their deep trap. It was also worth noting that long charge separation lifetimes are also beneficial in photocatalysis to effect degradation of organic pollutants. Overall, the quantitative determination of the concentration of thioanisole radical cation when photolysing MOF-5 and P25 TiO_2 under the same conditions constitutes strong evidence that the efficiency of MOF-5 acting as a semiconductor can be higher than that of the most widely used titania semiconductor.

The above photophysical data demonstrate that upon light absorption, MOF-5 undergoes charge separation. Calculations based on Marcus formalism have revealed that the reorganization energy for the hole transfer from the MOF-5 charge separated state to one electron donor is 1.2 times higher than the same parameter for ZnO.[49,69] This high reorganization energy indicates a significant structural change in the metal–ligand distance, binding strength and bond angles in the process.[70] This is not totally unexpected considering that the framework of MOFs is known to exhibit a high flexibility to accommodate the framework to the conditions and circumstances experienced by the material. Depending on the conditions as well as the presence of solvent molecules or guests significant structural changes have been observed. What are new are the data about the energetic cost of the reorganization of each site.

8. Laser flash photolysis of hydrated MOF-5

As mentioned in Section 2 when presenting the structure of MOFs, one of the most important drawbacks of MOFs is their relatively low structural stability. This poor crystal stability is particularly problematic in the case of MOF-5. It has been reported that the crystal structure of MOF-5 changes spontaneously to a different one termed as MOF-5′ upon mere exposure to moisture or storage in the open atmosphere.[71]

In this context, an interesting observation is that the photoluminescence of MOF-5 suspended in water undergoes a remarkable blue-shift (λ_{em} from 535 to 440 nm), accompanied by a change in the corresponding excitation spectrum and a shortening of the lifetime to 5 ns.[49] These changes in the photoluminescence spectrum have been proposed to originate from the structural transformation produced by water that converts MOF-5 to MOF-5′ material.[45,72] This is clearly demonstrated by the observation of a change in the XRD pattern of the solid as reported in the literature.[71] In this context we have also commented that not surprisingly emission and excitation spectra of MOF-5 undergo remarkable variations upon the phase change from MOF-5 to the resulting hydrated MOF-5′. This phase transformation has been attributed to the partial hydrolysis of the Zn carboxylate bond as indicated in Scheme 7 and is also reflected by variations in λ_{em}.[71]

As mentioned earlier, MOF-5 is unstable when stored under moist air or upon stirring in aqueous suspension. The above change in the MOF-5 structure in the presence of humidity makes some data in the literature uncertain as to whether they correspond to MOF-5 or to the resulting material after transformation. In this sense Majima and co-workers have established the transient diffuse reflectance spectra of hydrated MOF-5.[49] This optical spectrum exhibits two maxima around 480 and 740 nm decaying with the same temporal profile (Fig. 15).

No assignment of these peaks has been yet proposed. However these authors clearly established that upon photoexcitation of hydrated MOF-5 the material can participate also in photoinduced electron transfer processes in the presence of electron donor or electron acceptor quenchers. Thus, if hydrated MOF-5 is photolysed in the presence of triethylamine a peak at 550 nm attributable to terephthalic acid radical cation is recorded while if hydrated MOF-5 is irradiated in the presence of methyl viologen (MV^{2+}) the corresponding MV radical cation is detected (Fig. 16).

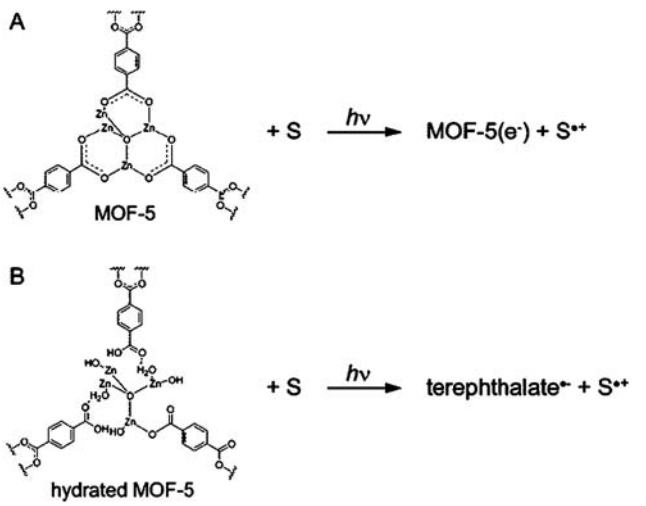

Scheme 7 Photoinduced one-electron oxidation of S on unhydrated (A) and hydrated (B) MOF-5 nanoparticles. (Taken from ref. 49 with permission.)

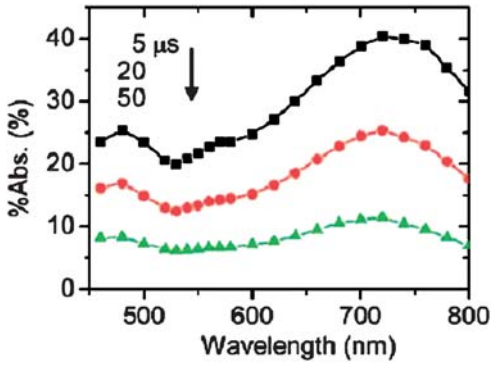

Fig. 15 Time-resolved diffuse-reflectance spectra observed at 5, 20 and 50 μs after the laser flash during 355 nm laser photolysis of the MOF-5 hydrated powder slurried in acetonitrile. (Figure taken from ref. 49 with permission.)

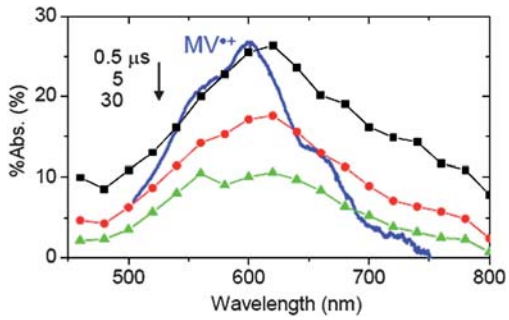

Fig. 16 Time-resolved diffuse-reflectance spectra observed at 0.5, 5 and 30 μs after the laser flash during the 355 nm laser photolysis of the MOF powder slurries in water (pH 7) in the presence of methyl viologen (MV^{2+}) (10 mM). The blue solid line indicates the absorption spectrum of $MV^{\bullet+}$ in water.[49,73] (Figure taken from ref. 49 with permission.)

Overall these observations indicate that even after phase transformation the resulting hydrated MOF-5 exhibits the typical behavior of a semiconductor being able to give and accept electrons depending on the nature of the quencher.

9. Trapping of photogenerated electrons and holes in MOF-5

When an aqueous suspension of MOF-5 containing $MVCl_2$ is illuminated with a solar simulator, generation of $MV^{\bullet+}$ is observed.[46] MV^{2+} and viologens in general have been widely used in photochemistry to trap electrons mainly because their corresponding radical cation can be easily detected and characterized by its typical optical spectrum.[74] In addition, in the absence of oxygen, viologen radical cations are long-lived intermediates that under certain circumstances can be even detected visually by their deep blue color. Considering the microporosity of MOF-5, it was assumed that viologens can diffuse from the solution to the internal voids of MOF where they can meet electrons being generated in the photoinduced charge separation process characteristic of semiconductors. Thus, when this aqueous suspension containing MV^{2+} and MOF-5 was irradiated, the blue color characteristic of $MV^{\bullet+}$ was observed.[46] Moreover, while the solution is colorless the blue color is observed in the solid

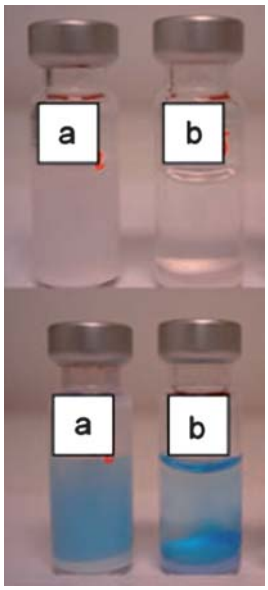

Fig. 17 Photographs showing a) P25 TiO_2 and b) MOF-5 solid samples in contact with aqueous solutions of methyl viologen dichloride, before (top) and after (bottom) irradiating with a solar simulator (525 W) through an AM1.5 filter for 10 min. (Figure taken from ref. 46.)

materials. Controls performing similar experiments with silica failed to generate $MV^{\bullet+}$. In contrast, when analogous experiments were performed using TiO_2, similar behaviour to that occurring in MOF was observed. Fig. 17 shows some photographs in which the blue color of $MV^{\bullet+}$ can be seen.

Generation of $MV^{\bullet+}$ by irradiation of aqueous suspensions of MOF-5 was interpreted as indicative of the quenching of electrons generated in MOF by viologen. Scheme 8 summarizes the proposed mechanism.[46]

Similarly, photoinduced holes generated in MOF-5 could be quenched by *N*,*N*,*N*′,*N*′-tetramethyl-*p*-phenylenediamine (PDA). This aromatic diamine is a good electron donor for positive holes and upon electron transfer generates the corresponding radical cation that similarly to viologen radical cation also exhibits an intense blue color. Again, amorphous silica, an insulator material, does not form phenylenediamine radical cation that is however observed when TiO_2, instead of MOF-5, is present in the suspension. Fig. 18 shows a photograph in which the characteristic blue color of phenylenediamine radical cation can be visually observed under certain conditions.

Scheme 9 shows the most likely mechanism to rationalize the observed formation of phenylenediamine radical cation from hole trap.

These simple electron and hole trapping experiments using well-known electron acceptor (viologen) or electron donor (phenylenediamine) compounds and visual observation of the corresponding radical cations unambiguously prove the behavior

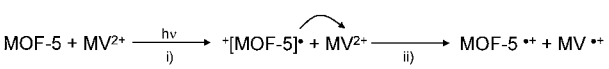

Scheme 8 Photochemical process leading to the generation of $MV^{\bullet+}$: i) photoinduced charge separation; ii) electron transfer.[46]

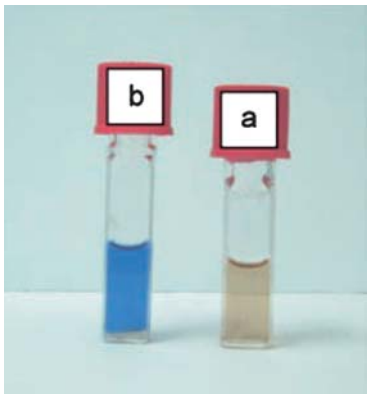

Fig. 18 Photograph showing a deaerated solution of *N*,*N*,*N*′,*N*′-tetramethyl-*p*-phenylenediamine in a) the absence and b) the presence of MOF-5 upon 355 nm laser irradiation. (Figure taken from ref. 46.)

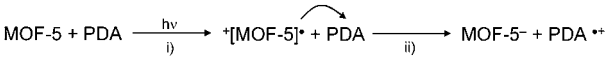

Scheme 9 Photochemical process leading to the generation of phenylenediamine radical cation ($PDA^{\bullet+}$): i) photoinduced charge separation; ii) electron transfer.

of MOF-5 as a semiconductor because they show that the same material upon photoirradiation is able to produce oxidation (phenylenediamine) and reduction (methyl viologen), dual behavior that arises from photoinduced charge separation with simultaneous formation of electron and holes and that is characteristic of semiconductors.

10. Energy levels in MOF-5

The bandgap of MOF-5 estimated from the diffuse reflectance optical spectrum was 3.4 eV. This value of bandgap energy is somewhat higher than, but similar to, that of TiO_2 anatase and shows that MOF-5 is a wide bandgap semiconductor (Scheme 10). The energy of the conduction band edge has been indirectly estimated by comparing the open-circuit voltages of a photovoltaic cell using MOF-5 as semiconductor and I_2/I^- as electrolyte with a second one prepared analogously with TiO_2. Since the electrolyte and its concentration were the same in both cells and the open-circuit voltage reflects the difference in energy between the electrolyte and the edge of the semiconductor conduction band, it should be possible to estimate the position of the conduction band with respect to that of TiO_2.

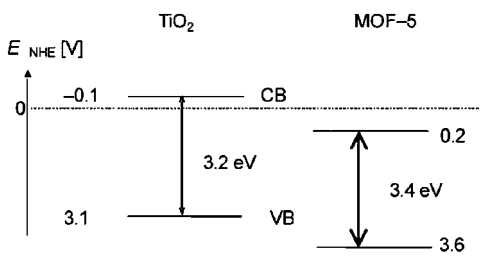

Scheme 10 Calculated values of the band gap and position of the conduction and valence band for MOF-5 in comparison with those of TiO_2. (Figure taken from ref. 46.)

The data presented in Scheme 10 show that electrons in the MOF-5 conduction band are 0.3 eV less reductants than in the conduction band of TiO_2. However, the above estimation is based on the assumption that the internal resistance of the two photovoltaic cells made of TiO_2 or MOF-5 is identical, an assumption that should be checked. Thus, it appears convenient to confirm the flat band potentials of MOF-5 by alternative techniques.

According to these energy values, MOF-5 should be a strongly oxidizing semiconductor. However, the reduction potential of the electrons in the conduction band of MOF-5 should be very low. Thus, MOF-5 as a semiconductor should not be able to generate H_2 from H_2O upon photoirradiation since this process, corresponding to a semireaction in the overall water splitting, would require an E_{red} value of 0 V plus an overpotential. In this context water splitting is an emerging field of application for semiconductors and these data apparently rule out the use of MOF-5 for this purpose.

11. Photocatalytic activity of MOFs

One of the most common applications of semiconductors is in photocatalysis where a solid converts light into chemical energy. The most common application of photocatalysis is the oxidative degradation of organic compounds in the gas or aqueous phase.[75–78] It has been proposed that the photocatalytic activities for the degradation of organic compounds by different materials should be compared using the degradation of phenol as a model for aromatic compounds.[79,80] By irradiating through pyrex an aerated suspension of phenol in the presence of a solid photocatalyst phenol becomes converted to hydroquinone and catechol and eventually the transformation progresses to, at least partial, oxidative degradation to CO_2 and H_2O.

Having established the behavior of MOF-5 as a semiconductor, a logic step forward has been to test its photoactivity towards the degradation of phenol. Fig. 19 shows the temporal evolution of the phenol degradation when this pollutant is submitted to irradiation through pyrex in aerated suspensions containing MOF-5, P25 TiO_2 or ZnO.[46]

The reason to compare these three materials is that zinc oxide should be the closest semiconductor in the case that the structure

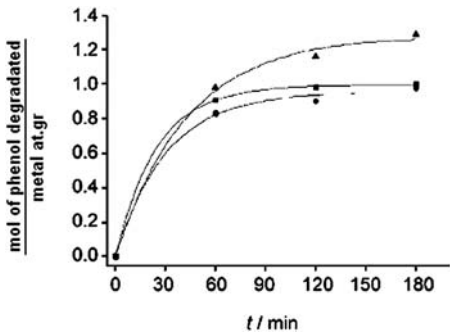

Fig. 19 Time conversion plots of phenol disappearance per metal atom in the presence of MOF-5 (-▲-),P25 TiO_2 (-■-) and ZnO (-●-) upon Hg lamp irradiation through pyrex. (Figure taken from ref. 46.)

of MOF-5 collapses during the experiment in aqueous medium, while P25 TiO_2 is the benchmark photocatalyst to which the other photocatalysts should be compared. Blank controls under the same conditions in the absence of any photocatalyst showed no degradation of phenol. As can be seen in Fig. 19, MOF-5 shows a significant photocatalytic activity that when plotted per metal atom is even higher than that exhibited by P25 or ZnO. However, this type of comparison is misleading since the structures and compositions of the materials are very different and it can be cumbersome to agree on a single parameter (weight, surface are, metal content) for the comparison. In any case the phenol degradation plot shown in Fig. 19 indicates a remarkable photocatalytic activity of MOF-5 that, depending on the figure of merit used in the comparison, can be even higher than that of P25 TiO_2.

Besides degradation of organic pollutants (*negative photocatalysis*) another aspect would be to develop photocatalysts for the light-assisted synthesis of valuable organic compounds (*positive photocatalysis*). In this field, the groups of Kapteijn and Mul have reported recently an *in operando* FTIR study of the use of isoreticular MOFs as tunable bandgap photocatalysts for the efficient oxidation of propylene to acetone and propionic acid (Scheme 11).[81] In this regard, photocatalysis, as an efficient way to activate molecular oxygen, could be and alternative technology for catalytic aerobic oxidations.

One pre-requisite for the use of a solid in photochemical applications is its photostability upon prolonged exposures to light. Light stability is certainly an important issue that has been mostly ignored when pursuing the use of MOFs as semiconductors. Taking into account that one of the major applications of ZnO, TiO_2 and other semiconductors is the photocatalytic degradation of organic compounds and that MOFs contain an organic linker, the photostability of MOFs should be submitted to a survey. Also, as we have mentioned, MOFs are in general not very stable upon thermal or chemical treatment as well as upon exposure to moisture or other solvents. In the case of MOF-5 irradiation of powdered samples with the pyrex filtered output of a 1 kW mercury lamp for 5 h did not lead to any observable change in the X-ray diffractogram before and after irradiation. This fact rules out the occurrence of photochemically promoted structure collapse as it should occur if photodecarboxylation or any other photochemical damage of the terephthalate ligand would take place massively.

However, considering that XRD is biased towards crystalline materials and that the sensitivity of quantitative XRD is not very high, it could have been that photodegradation has occurred to a minor extent, the consequences of this damage being only apparent for very long irradiation times. Certainly a deeper study on the photochemical stability for a series of MOFs will be highly valuable to ensure the long-term applicability of MOFs in optoelectronic systems.

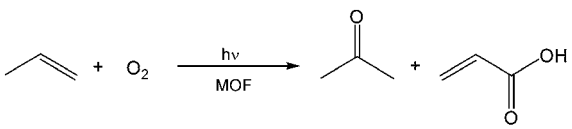

Scheme 11 Photo-oxidation of propylene to acetone and propionic acid using a MOF as photocatalyst.

12. Application of MOF-5 in photovoltaic and electroluminescence cells

The previous sections have presented the current evidence supporting that MOFs exhibits the characteristic behavior of semiconductors, *i.e.*, generation of electrons and holes upon photoexcitation with light of energy larger than their bandgap. Direct detection of electrons and holes or their trapping constitute firm proof of MOF's semiconductor nature. In view of these data, it can be presumed that MOFs could be useful for those applications based on the use of semiconductors. Photocatalysis directed to the degradation of undesirable organic pollutants is one of these general applications of semiconductors. We have already commented on the photocatalytic activity of MOF-5 for phenol degradation. Other typical and technologically important applications will be the use of MOFs in photovoltaic cells and electroluminescence diodes.

As we have mentioned earlier, the energy values of the conduction and valence bands of MOF-5 have been indirectly estimated from the open-circuit potential of a photovoltaic cell. Actually, to prove the concept of the use of MOF-5 as an active semiconductor layer, an unoptimized photovoltaic cell based on a thin film of MOF-5 without a light harvester dye has been tested.[82] Upon illumination with a solar simulator, photocurrent from a cell based on MOF-5 has been observed. The *I–V* curve obtained for the MOF-5 solar cell under irradiation with an AM1.5-filtered solar light simulator is shown in Fig. 20. Efficiency data obtained from this response of the photovoltaic cell were V_{OC} 0.33 V, I_{SC} 0.7 μA, and FF 44%. Although these values are much lower than those obtained using conventional P-25 titania under exactly the same conditions (V_{OC} 0.52 V, I_{SC} 209 μA, and FF 58%), they should be considered promising due to the large flexibility in the choice of possible MOFs and the possibility to introduce light harvesting dyes. The large surface area and pore volume of MOFs make these materials especially suitable to incorporate a large quantity of light-harvesting dye that would have a large interfacial area to interact with semiconductor and electrolyte. In any case, the intrinsic photovoltaic response observed for MOF-5 also proves indirectly its

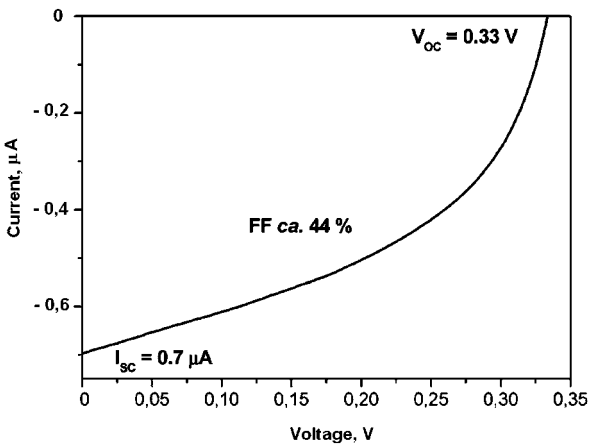

Fig. 20 *I–V* curve obtained for the photovoltaic solar cell prepared with MOF-5 upon irradiation with an AM1.5-filtered lamp (525 W) using an ITO-glass electrode. (Figure taken from ref. 82.)

semiconductor properties. This behavior of MOF-5 contrasts with zeolites that do not show any photovoltaic activity upon illumination.

Thin films of MOF-5 also behave as phosphors. The basic structure of an inorganic electroluminescent device is similar to that of the photovoltaic cell described above, since the fundamental phenomena occurring in both types of cells are the reverse of each other. In a photovoltaic cell illumination of the semiconductor films originates the build up of a current, while phosphors emit light when they are submitted to an electrical current.

As expected in view of the mentioned behavior of MOF-5 as a semiconductor, MOF-5 submitted to an alternating current (180 Hz) of 60 V emits light. The emission spectrum of MOF-5 is shown in Fig. 21 and consists of a broad (fwhm 135 nm) and quasi-symmetric band, with a small shoulder on the high-energy side. From this spectrum, a value of about 565 nm was derived for $\lambda_{EL(max)}$, which is very close to the value of 540 nm obtained for the corresponding photoluminescence emission maximum. Ideally, photoluminescence and phosphor emission spectra should coincide when they involve the same transient species. The difference between these two techniques is in the generation of the electronically excited state that occurs through electron/hole recombination in the case of electroluminescence or by light excitation for photoluminescence. Other analogous non-crystalline metal organic materials constituted by tin-terephthalate also behave similarly to MOF-5 and emit light under similar conditions as those used for MOF-5. This observation suggests that crystal structure and microporosity is not a prerequisite for the observation of electroluminescence.

Although the efficiency of MOF-5 as a phosphor was also low, observation of this phenomenon on MOFs can serve again to trigger further research in this field trying to improve the performance of this family of materials for this application. In this context, rare earth metals have been widely used as structural metals in the synthesis of MOFs and considering their strong phosphorescence they are obvious candidates to be tested for this type of optoelectronic properties.

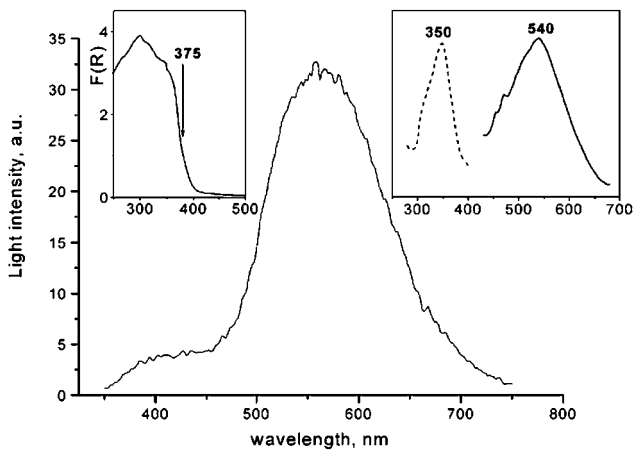

Fig. 21 Electroluminescence emission spectrum of MOF-5, obtained with a square ac voltage of 60 V and a frequency of 180 Hz. Left inset: Diffuse reflectance UV/Vis spectrum of MOF-5. The arrow marks the position of the inflection point of the absorption band (optical band gap). Right inset: Photoluminescence excitation (dashed line, monitored at 540 nm) and emission (full line, exciting at 350 nm) spectra of MOF-5. (Figure taken from ref. 82.)

13. Conclusions

The main purpose of this account has been to present evidence in support of the consideration of some MOFs as semiconductors. Currently the synthesis and characterization of MOFs is a research front in chemistry and materials science. The information gained on the synthesis indicates that there are a considerable number of predictive tools to prepare new MOFs. Some of the MOFs have been prepared by design to obtain materials with certain desirable properties. However the main application of MOFs is still as gas adsorbers, a field where the added value of the material is low compared to optoelectronics. Considering the versatility, ease of MOF preparation, availability and the important properties of semiconductors, our aim is to trigger specific research focused on the synthesis of task-specific MOFs specially conceived to enhance and improve their performance as semiconductors. In this area and in contrast to their use as heterogeneous catalysts, MOFs have already surpassed the performance of zeolites. Among the potential applications that MOFs as semiconductors would offer the most useful ones could be as shape selective photocatalysts for the selective degradation of organic compounds or for the synthesis of industrial compounds, for their use in photovoltaic devices tuned for solar cells, electroluminescent devices, field electron transistors and sensors. It is very likely that these fields will develop in the near future.

Acknowledgements

Financial support by the Spanish DGI (CTQ2009-11583) is gratefully acknowledged. Cláudia G. Silva thanks Fundação para a Ciência e a Tecnologia (Portugal) for the post-doctoral fellowship (SFRH/BPD/48777/2008).

References

1 H. v. Bekkum, E. M. Flanigen and J. C. Jansen, *Introduction to zeolite science and practice*, Elsevier, Amsterdam, 1991.
2 R. M. Barrer, *Zeolites and clay minerals as sorbents and molecular sieves*, Academic Press, London, 1978.
3 D. W. Breck, *Zeolite molecular sieves: Structure, chemistry and use*, John Wiley & Sons, New York, 1974.
4 M. E. Davis, *Acc. Chem. Res.*, 1993, **26**, 111–115.
5 M. E. Davis, *Chem.–Eur. J.*, 1997, **3**, 1745–1750.
6 A. Corma, *J. Catal.*, 2003, **216**, 298–312.
7 X. C. Meng, Y. X. Wu and Y. D. Li, *J. Porous Mater.*, 2006, **13**, 365–371.
8 A. Corma, M. J. Diaz-Cabanas, J. L. Jorda, C. Martinez and M. Moliner, *Nature*, 2006, **443**, 842–845.
9 A. Corma, M. Moliner, F. Rey and J. González, *Microporous crystalline material of zeolitic nature, zeolite ITQ-39, method of preparation and uses*, WO/2008/092984, 2008.
10 J. L. Sun, C. Bonneau, A. Cantin, A. Corma, M. J. Diaz-Cabanas, M. Moliner, D. L. Zhang, M. R. Li and X. D. Zou, *Nature*, 2009, **458**, 1154–U1190.
11 A. Corma and A. Martinez, in *Zeolites and Ordered Mesoporous Materials: Progress and Prospects - Studies in Surface Science and Catalysis*, ed. J. Cejka and H. Van Bekkum, Elsevier Science BV, Amsterdam, 2005, pp. 337–366.

12 B. Yilmaz and U. Muller, in *International Sympsium on Creation and Control of Advanced Selective Catalysis*, Springer/Plenum Publishers, Kyoto, JAPAN, 2008, pp. 888–895.
13 M. Alvaro, J. F. Cabeza, D. Fabuel, A. Corma and H. Garcia, *Chem.–Eur. J.*, 2007, **13**, 3733–3738.
14 M. Comes, M. D. Marcos, R. Martinez-Manez, M. C. Millan, J. V. Ros-Lis, F. Sancenon, J. Soto and L. A. Villaescusa, *Chem.–Eur. J.*, 2006, **12**, 2162–2170.
15 A. Corma, U. Diaz, B. Ferrer, V. Fornes, M. S. Galletero and H. Garcia, *Chem. Mater.*, 2004, **16**, 1170–1176.
16 A. Corma and H. Garcia, *Chem. Commun.*, 2004, 1443–1459.
17 A. Corma and H. Garcia, *Eur. J. Inorg. Chem.*, 2004, 1143–1164.
18 C. Leiggener and G. Calzaferri, *ChemPhysChem*, 2004, **5**, 1593–1596.
19 A. Walcarius, *Anal. Chim. Acta*, 1999, **384**, 1–16.
20 A. L. Garay, A. Pichon and S. L. James, *Chem. Soc. Rev.*, 2007, **36**, 846–855.
21 J. J. Perry, J. A. Perman and M. J. Zaworotko, *Chem. Soc. Rev.*, 2009, **38**, 1400–1417.
22 G. K. H. Shimizu, R. Vaidhyanathan and J. M. Taylor, *Chem. Soc. Rev.*, 2009, **38**, 1430–1449.
23 A. J. Fletcher, K. M. Thomas and M. J. Rosseinsky, *J. Solid State Chem.*, 2005, **178**, 2491–2510.
24 S. Natarajan and P. Mahata, *Chem. Soc. Rev.*, 2009, **38**, 2304–2318.
25 M. P. Suh, Y. E. Cheon and E. Y. Lee, *Coord. Chem. Rev.*, 2008, **252**, 1007–1026.
26 M. Kurmoo, *Chem. Soc. Rev.*, 2009, **38**, 1353–1379.
27 J. Lee, O. K. Farha, J. Roberts, K. A. Scheidt, S. T. Nguyen and J. T. Hupp, *Chem. Soc. Rev.*, 2009, **38**, 1450–1459.
28 J. R. Li, R. J. Kuppler and H. C. Zhou, *Chem. Soc. Rev.*, 2009, **38**, 1477–1504.
29 D. Maspoch, D. Ruiz-Molina and J. Veciana, *Chem. Soc. Rev.*, 2007, **36**, 770–818.
30 C. Z. Mu, F. Xu and W. Lei, *Prog. Chem.*, 2007, **19**, 1345–1356.
31 L. J. Murray, M. Dinca and J. R. Long, *Chem. Soc. Rev.*, 2009, **38**, 1294–1314.
32 B. V. Harbuzaru, A. Corma, F. Rey, J. L. Jorda, D. Ananias, L. D. Carlos and J. Rocha, *Angew. Chem., Int. Ed.*, 2009, **48**, 6476–6479.
33 M. Eddaoudi, D. B. Moler, H. L. Li, B. L. Chen, T. M. Reineke, M. O'Keeffe and O. M. Yaghi, *Acc. Chem. Res.*, 2001, **34**, 319–330.
34 S. L. James, *Chem. Soc. Rev.*, 2003, **32**, 276–288.
35 N. W. Ockwig, O. Delgado-Friedrichs, M. O'Keeffe and O. M. Yaghi, *Acc. Chem. Res.*, 2005, **38**, 176–182.
36 J. L. C. Rowsell and O. M. Yaghi, *Microporous Mesoporous Mater.*, 2004, **73**, 3–14.
37 M. Eddaoudi, J. Kim, N. Rosi, D. Vodak, J. Wachter, M. O'Keeffe and O. M. Yaghi, *Science*, 2002, **295**, 469–472.
38 H. Li, M. Eddaoudi, M. O'Keeffe and O. M. Yaghi, *Nature*, 1999, **402**, 276–279.
39 O. M. Yaghi, M. O'Keeffe, N. W. Ockwig, H. K. Chae, M. Eddaoudi and J. Kim, *Nature*, 2003, **423**, 705–714.
40 M. D. Allendorf, C. A. Bauer, R. K. Bhakta and R. J. T. Houk, *Chem. Soc. Rev.*, 2009, **38**, 1330–1352.
41 M. Fuentes-Cabrera, D. M. Nicholson, B. G. Sumpter and M. Widom, *J. Chem. Phys.*, 2005, **123**, 124713.
42 Z. D. Lu, L. L. Wen, Z. P. Ni, Y. Z. Li, H. Z. Zhu and Q. J. Meng, *Cryst. Growth Des.*, 2007, **7**, 268–274.
43 S. Bordiga, C. Lamberti, G. Ricchiardi, L. Regli, F. Bonino, A. Damin, K. P. Lillerud, M. Bjorgen and A. Zecchina, *Chem. Commun.*, 2004, 2300–2301.
44 S. Monticone, R. Tufeu and A. V. Kanaev, *Chem. Phys. Lett.*, 1998, **295**, 237–244.
45 S. Monticone, R. Tufeu and A. V. Kanaev, *J. Phys. Chem. B*, 1998, **102**, 2854–2862.
46 M. Alvaro, E. Carbonell, B. Ferrer, F. Xamena and H. Garcia, *Chem.–Eur. J.*, 2007, **13**, 5106–5112.
47 N. J. Turro, V. Ramamurthy and J. C. Scaiano, *Principles of Molecular Photochemistry: An Introduction*, University Science Books, Sausalito, CA, 2008.
48 S. Corrent, G. Cosa, J. C. Scaiano, M. S. Galletero, M. Alvaro and H. Garcia, *Chem. Mater.*, 2001, **13**, 715–722.
49 T. Tachikawa, J. R. Choi, M. Fujitsuka and T. Majima, *J. Phys. Chem. C*, 2008, **112**, 14090–14101.
50 H. J. Egelhaaf and D. Oelkrug, *J. Cryst. Growth*, 1996, **161**, 190–194.
51 C. A. Bauer, T. V. Timofeeva, T. B. Settersten, B. D. Patterson, V. H. Liu, B. A. Simmons and M. D. Allendorf, *J. Am. Chem. Soc.*, 2007, **129**, 7136–7144.
52 Z. F. Chen, R. G. Xiong, J. Zhang, X. T. Chen, Z. L. Xue and X. Z. You, *Inorg. Chem.*, 2001, **40**, 4075–4076.
53 B. Civalleri, F. Napoli, Y. Noel, C. Roetti and R. Dovesi, *CrystEngComm*, 2006, **8**, 364–371.
54 M. Alvaro, V. Fornes, S. Garcia, H. Garcia and J. C. Scaiano, *J. Phys. Chem. B*, 1998, **102**, 8744–8750.
55 J. L. Adam, *Chem. Rev.*, 2002, **102**, 2461–2476.
56 B. L. Chen, L. B. Wang, Y. Q. Xiao, F. R. Fronczek, M. Xue, Y. J. Cui and G. D. Qian, *Angew. Chem., Int. Ed.*, 2009, **48**, 500–503.
57 B. L. Chen, Y. Yang, F. Zapata, G. N. Lin, G. D. Qian and E. B. Lobkovsky, *Adv. Mater.*, 2007, **19**, 1693.
58 B. V. Harbuzaru, A. Corma, F. Rey, P. Atienzar, J. L. Jorda, H. Garcia, D. Ananias, L. D. Carlos and J. Rocha, *Angew. Chem., Int. Ed.*, 2008, **47**, 1080–1083.
59 T. Justel, H. Nikol and C. Ronda, *Angew. Chem., Int. Ed.*, 1998, **37**, 3084–3103.
60 K. Kuriki, Y. Koike and Y. Okamoto, *Chem. Rev.*, 2002, **102**, 2347–2356.
61 S. I. Klink, L. Grave, D. N. Reinhoudt, F. van Veggel, M. H. V. Werts, F. A. J. Geurts and J. W. Hofstraat, *J. Phys. Chem. A*, 2000, **104**, 5457–5468.
62 Y. Kim, M. Suh and D. Y. Jung, *Inorg. Chem.*, 2004, **43**, 245–250.
63 F. Millange, C. Serre, J. Marrot, N. Gardant, F. Pelle and G. Ferey, *J. Mater. Chem.*, 2004, **14**, 642–645.
64 T. M. Reineke, M. Eddaoudi, M. Fehr, D. Kelley and O. M. Yaghi, *J. Am. Chem. Soc.*, 1999, **121**, 1651–1657.
65 C. Serre, F. Millange, C. Thouvenot, N. Gardant, F. Pelle and G. Ferey, *J. Mater. Chem.*, 2004, **14**, 1540–1543.
66 R. G. Xiong, J. Zhang, Z. F. Chen, X. Z. You, C. M. Che and H. K. Fun, *J. Chem. Soc., Dalton Trans.*, 2001, 780–782.
67 F. Gandara, A. Garcia-Cortes, C. Cascales, B. Gomez-Lor, E. Gutierrez-Puebla, M. Iglesias, A. Monge and N. Snejko, *Inorg. Chem.*, 2007, **46**, 3475–3484.
68 P. V. Kamat and M. A. Fox, *Chem. Phys. Lett.*, 1983, **102**, 379–384.
69 T. Yago, Y. Kobori, K. Akiyama and S. Tero-Kubota, *Chem. Phys. Lett.*, 2003, **369**, 49–54.
70 A. Janotti and C. G. Van de Walle, *Appl. Phys. Lett.*, 2005, **87**, 122102.
71 J. A. Greathouse and M. D. Allendorf, *J. Am. Chem. Soc.*, 2006, **128**, 10678–10679.
72 T. J. Mason, J. P. Lorimer, D. M. Bates and Y. Zhao, *Ultrason. Sonochem.*, 1994, **1**, S91–S95.
73 T. N. Das, T. K. Ghanty and H. Pal, *J. Phys. Chem. A*, 2003, **107**, 5998–6006.
74 M. Alvaro, H. Garcia, S. Garcia, F. Marquez and J. C. Scaiano, *J. Phys. Chem. B*, 1997, **101**, 3043–3051.
75 M. R. Hoffmann, S. T. Martin, W. Y. Choi and D. W. Bahnemann, *Chem. Rev.*, 1995, **95**, 69–96.
76 A. Mills, R. H. Davies and D. Worsley, *Chem. Soc. Rev.*, 1993, **22**, 417–425.
77 A. Mills and S. LeHunte, *J. Photochem. Photobiol., A*, 1997, **108**, 1–35.
78 J. Peral, X. Domenech and D. F. Ollis, *J. Chem. Technol. Biotechnol.*, 1997, **70**, 117–140.
79 A. Salinaro, A. V. Emeline, J. C. Zhao, H. Hidaka, V. K. Ryabchuk and N. Serpone, *Pure Appl. Chem.*, 1999, **71**, 321–335.
80 N. Serpone and A. Salinaro, *Pure Appl. Chem.*, 1999, **71**, 303–320.
81 J. Gascon, M. D. Hernandez-Alonso, A. R. Almeida, G. P. M. van Klink, F. Kapteijn and G. Mul, *ChemSusChem*, 2008, **1**, 981–983.
82 F. Xamena, A. Corma and H. Garcia, *J. Phys. Chem. C*, 2007, **111**, 80–85.

